Fully 3D-Printed, Monolithic, Mini Magnetic Actuators for Low-Cost, Compact Systems

Anthony P. Taylor, Camilo Vélez Cuervo, *Member, IEEE*, David P. Arnold, *Senior Member, IEEE*, and Luis Fernando Velásquez-García, *Senior Member, IEEE*

***Abstract*— We report the design, fabrication, and experimental characterization of the first fully 3D-printed, multi-material miniature magnetic actuators for compact systems in the literature. The actuator design integrates a bonded hard magnet made of NdFeB microparticles embedded in a Nylon 12 matrix (55% by volume) with structural and support elements made of pure Nylon 12. The device is a 10 mm-diameter, 1.2 mm wall-thick, and 9 mm tall cylindrical frame that mounts on an off-the-shelf solenoid and a 10 mm diameter, 100 μm-thick, leak-tight membrane connected at its center to a 4 mm diameter, 4.95 mm tall hard magnet. The actuators are monolithically printed in layers as thin as 100 μm using 600 μm-wide strokes via fused filament fabrication (FFF) –a low-cost 3D printing technology capable of processing high-performance thermoplastics to create monolithic objects made of a plurality of distinctive feedstock. The average surface roughness, Young's modulus, and hardness of the FFF-printable hard-magnetic filament were estimated at 58.55 μm, 3.59 GPa, and Shore D 71.5, respectively, while the average surface roughness, Young's modulus, and yield strength of FFF-printed magnetic material were estimated at 5.79 μm, 2.02 GPa, and 55.99 MPa ± 4.59 MPa, respectively. Magnetic characterization of the FFF-printed NdFeB-embedded Nylon 12 feedstock demonstrates the fabrication of isotropic hard magnets with an intrinsic coercivity of ∼700 kA/m, remanence of ∼395 mT, and a maximum energy product of 27 kJ/m^3. Simulations of the stray magnetic field produced by a printed sample made of NdFeB-embedded Nylon 12 were validated using a scanning Hall probe. The vertical displacement of a miniature 3D-printed magnetic actuator was characterized with a solenoid for various coil bias voltages; a maximum displacement equal to 50 μm was obtained with 3.1 V DC applied to the driving coil. Finite element simulations of the actuator design estimate at 2.38 MPa the maximum stress on the membrane at 50 μm actuation (i.e., below the fatigue limit of Nylon 12), and at 592.61 Hz the natural frequency of the device, which was corroborated via experiment. [2018-0288]**

***Index Terms*— 3D printing of MEMS, bonded hard magnet, fused filament fabrication, magnetic actuator, monolithic multi-material 3D printing of microsystems.**

Manuscript received December 2, 2018; revised February 26, 2019; accepted April 5, 2019. Date of publication April 26, 2019; date of current version May 31, 2019. This work was supported in part by Edwards Vacuum. Subject Editor S. M. Spearing. *(Corresponding author: Luis Fernando Velásquez-García.)*

A. P. Taylor is with Edwards Vacuum, Sanborn, NY 14132 USA, and also with the Massachusetts Institute of Technology, Cambridge, MA 02139 USA (e-mail: anthony.taylor@edwardsvacuum.com).

C. Vélez Cuervo and D. P. Arnold are with the Interdisciplinary Microsystems Group (IMG), Electrical and Computer Engineering Department, University of Florida, Gainesville, FL 32611-6200 USA (e-mail: camilovelez@ufl.edu; darnold@ufl.edu).

L. F. Velásquez-García is with the Microsystems Technology Laboratories, Massachusetts Institute of Technology, Cambridge, MA 02139 USA (e-mail: velasquez@alum.mit.edu).

Color versions of one or more of the figures in this paper are available online at http://ieeexplore.ieee.org.

Digital Object Identifier 10.1109/JMEMS.2019.2910215

I. Introduction

COMPACT analytical instruments (e.g., portable mass spectrometers [1], [2]) and other microsystems require a supply of liquids and/or gases at precise flow rates and pressure levels; this can be effectively implemented using miniaturized pumps that involve valves, pistons, bellows, and other actuators [3]–[5]. There are reports of miniaturized actuators that exploit piezoelectric [6], electrostatic [7], pneumatic [8], and electromagnetic [9] transduction; the latter mechanism is of interest for implementing fast actuation with large force and large displacement in a compact form factor, e.g., to drive compressible gas pumps [10]–where the ultimate pressure is directly related to the compression ratio of the pump chamber.

Additive manufacturing (AM) are bottom-up, layer-by-layer fabrication techniques that create solid objects described by a computer-aided design (CAD) digital model [11]. AM has unique advantages over traditional manufacturing such as freeform compatibility, fast design iteration, print-to-print customization, waste reduction, and cost reduction when producing complex parts, e.g., objects with hierarchical structure [12]. AM also makes possible to implement microsystems that are difficult, impractical, or unfeasible to make with standard microfabrication methods, e.g., monolithic multi-level microfluidics [13]–[16].

An active line of research on AM is the demonstration of multi-material, monolithic structures that are active, i.e., have embedded transducing components [17]. The goal of printing a multi-material device is to optimize the performance of its different parts via specialization (e.g., a device structure that is meant to accomplish a certain task should be made of a material with the right physical properties); the objective of printing the device monolithically is to avoid assembly of components and attain better integration to perhaps yield better performance. In particular, there has been a significant interest to integrate soft- and hard-magnetic materials in bonded magnets; however, the state of the art in AM and injection molding can offer only large-scale magnets [18], [19]. Small-scale magnets have been developed for microelectromechanical systems (MEMS) using bonded magnetic powders in photoresist and polymers [20]; Figure 1 summarizes the state of the art of macro- and micro-scaled bonded magnets, reporting three key properties of permanent magnets, i.e., intrinsic coercivity, remanence, and maximum energy product. Several research groups have pursued the demonstration of miniaturized actuators using bonded magnets and structural materials; in this effort, 3D printing technologies such as

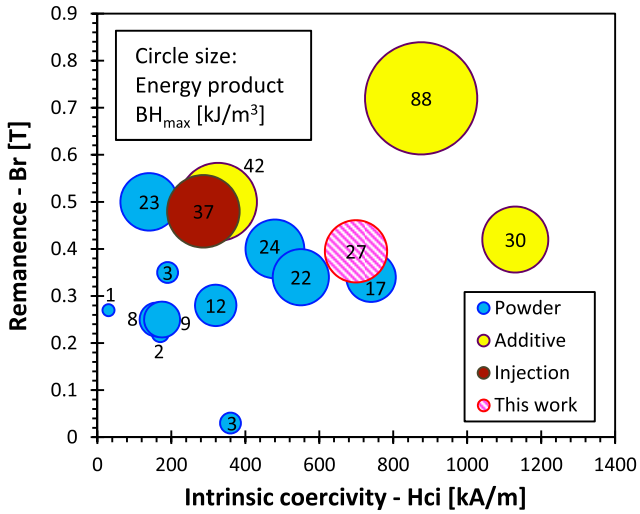

Fig. 1. Magnetic remanence (vertical axis), intrinsic coercivity (horizontal axis), and maximum energy product (circle size) of reported micro-scale and macro-scale bonded magnets [18]–[20].

digital light projection stereolithography (DLP-SLA), direct ink-writing (DIW), and fused filament fabrication (FFF) have been employed. However, the possibility of monolithically incorporating hard-magnetic components into finely featured structures made of high-performance plastics has not been fully realized:

- Using a modified DLP-SLA printer, flexible photo-curable resins reinforced with Fe_3O_4 magnetic nanoparticles have been monolithically printed in combination with the unmodified resin to build an actuator [21]. However, during printing, to switch from one material to another, the part has to be moved from one bath containing the pure resin to another bath containing the magnetically fortified resin; this can only be accomplished once to avoid contamination of the pure resin vat (or it requires as many fresh resin vats as there are different printed layers). Furthermore, only stratified parts can be made with this method (i.e., an object can only have a vertically layered structure that contains a single material in any given layer).
- Custom-designed DIW multi-material printers have been used to produce NdFeB bonded magnets in a silicone rubber matrix (up to 20% by volume), where a pulsed magnetic field is applied during printing to create ferromagnetic domains of different orientation within the object [22]. These parts are monolithically printed out of the magnetic resin and a support material also based on silicone rubber; the parts are then cured by heating them to 120 °C for 1 hr.; finally, the support material is dissolved in isopropanol.
- Using a commercial four-nozzle DIW printer, functional devices containing structural material with aligned, embedded magnetic particles, pure structural material, and flexible components were monolithically fabricated [23]. The inks used required photo-assisted curing; the magnetic ink contained a rather modest amount of Fe_3O_4 nanoparticle-coated alumina platelets (1% by weight). The platelets were aligned within the matrix using an external magnetic field; platelet alignment changed anisotropically the mechanical properties of regions in the printed parts, allowing for the design of shape-change materials.
- There are recent reports of FFF-printed bonded hard magnets using NdFeB microparticles embedded in Nylon 11 and 12 [24], [25]; composite polymer-soft magnetic materials have also been printed using FFF technology [26].

This study reports the first proof-of-concept demonstration of functional, compact, fully 3D-printed, monolithic magnetic actuators; the devices are composed of a hard magnet monolithically printed on top of a 100 μm-thick membrane held by a rigid frame. Compared to our earlier work on additively manufactured magnetic actuators with embedded off-the-shelf SmCo magnets [27], the new actuators have a membrane that is 33% thinner and occupies 86% less area; in addition, the new devices have a 3D-printed hard magnet monolithically integrated to the rest of the actuator. To achieve this, a hard-magnetic filament compatible with FFF printing was created, and a printing method that allows for precise dimensional control of magnetic components printed using such feedstock was developed. The hard-magnetic filament was extruded from commercial magnetic compound pellets used to make bonded magnets; the pellets are made of NdFeB ceramic magnetic microparticles embedded in a Nylon 12 polymer matrix. The produced printed magnets have stronger magnetic remanence (B_r) by nearly 30% and higher density by up to 18% compared to previously reported work on FFF-printed magnets [24], [25]. In addition, compared to reported DIW-printed magnets [22], our devices do not require curing, have much higher volume fraction of magnetic microparticles embedded in the polymer matrix, and incorporate a high-performance plastic (Nylon 12) in structural elements and flexible membranes for actuation. Moreover, unlike DLP-SLA-printed magnetic actuators [21], our device design is not constrained to a stratified material composition. The choice of NdFeB as magnetic material poses some trade-offs; compared to hard ferrites, NdFeB has significantly better magnetic properties, but is more expensive and less corrosion resistant [20]; compared to SmCo, NdFeB has better magnetic properties at low temperature (up to ~150 °C [28]) and is less expensive, but has less chemical stability and cannot operate at high temperatures (SmCo magnets can operate up to 550 °C [29]). Section II describes the printing method, fabrication, and characterization of printable magnetic feedstock, as well as the characterization of the printed magnetic material. Section III describes the design and fabrication of the proof-of-concept mini magnetic actuators. Section IV describes the structural device simulations, while Section V reports and discusses the experimental results. Section VI summarizes the work.

II. AM Method, Characterization of Printable Magnetic Material

A. AM Method

In this study, a CreatBot DX Plus FFF 3D printer (Henan Suwei Electronics Tech., Zhengzhou City, China) was used

to manufacture test structures and devices. The FFF method, based on extrusion of thermoplastic polymers [30], offers three key advantages over competing additive manufacturing technologies: (i) FFF is arguably the simplest printing method with the cheapest associated hardware and feedstock, (ii) FFF can print high-performance plastics, e.g., Nylon, PEEK, as feedstock to create truly functional objects, and (iii) FFF is a technology readily capable of printing freeform objects that are monolithically made of a plurality of distinctive feedstock [31]. The FFF printer has three 600 μm-diameter stainless steel extrusion nozzles arranged in a straight line accepting 2.85 mm-diameter filaments for multi-material printing. Commercially available Nylon 12 filament (Orbi-Tech, Leichlingen, Germany) and home-made NdFeB microparticle-doped Nylon 12 filament were extruded at 250 °C using the outer two nozzles, leaving a spacing of 40 mm between active nozzles that allows for nozzle interference-free printing of parts with in-plane (i.e., parallel to the plane of the build plate, or parallel to the printed layers) dimensions up to 40 mm. It is best practice to minimize interference between the nozzles and the printed part; interaction between an inactive extrusion nozzle and the printed object may result in unwanted localized melting, denting/scratching of the printed part, material oozing, and contamination of the material already printed or at the nozzle. The two active nozzles are leveled by adjusting their heights in the out-of-plane direction (i.e., perpendicular to the plane of the build plate, or perpendicular to the printed layers), and the third nozzle, located between the two active nozzles, is retracted by about 300 μm to avoid interfering with the printed object. The precise relative position between the active nozzles in the in-plane directions is estimated by measuring printed test structures; any differences between actual and nominal values are compensated by introducing global offsets in the printing software. The printer has a glass bed that is coated with a thin layer of polyvinyl acetate (PVAc) adhesive before printing to promote adhesion of the object to the bed. The printer is housed in a 3DPrintClean Model 600 enclosure (Mountainside NJ, USA) with recirculating HEPA filtration.

To print an object via FFF, a CAD model in *stl* format is created (SolidWorks 2015, Dassault Systèmes, Waltham MA, USA) and exported to a slicer software (Simplify3D, Cincinnati OH, USA), which transforms the 3D model into a set of horizontal cuts, i.e., *slices*, creating a *gcode* file that contains the traveling path that rasters each slice with associated conditions (e.g., nozzle temperature, bed temperature, filament feed rate, nozzle speed). The gcode file is then transferred to the 3D printer using a flash memory card, and the object is printed following the instructions of the gcode file. Finally, the print is carefully removed from the built plate using a utility knife blade and applying isopropanol to loosen the part from the bed.

B. Fabrication and Characterization of Magnetic Filament

Even though there are commercially available soft-magnetic filaments [32] (iron microparticles embedded in a PLA polymer matrix with ~11.5% volume concentration [33]), to the best of our knowledge there are no commercial hard-magnetic filaments suitable for FFF 3D printing. We first looked into making the hard-magnetic filament from raw materials, i.e., polymer pellets and finely ground hard-magnetic powder; however, this approach proved unfeasible due to the serious health and safety hazards associated to handling, storing, and processing these powders. Instead, the filament used to manufacture the magnets employed in this study was created using commercial pellet feedstock for bonded hard magnets supplied by Mate Corporation (Okayama, Japan). The vendor has available hard-magnetic compound pellets in a range of formulations, using Sr ferrite, SmCo, or NdFeB as magnetic filler and Nylon 12 or polyphenylene sulfide (PPS) as binder, with different magnetic, mechanical, chemical, and heat resistant properties; the magnet microbeads are typically on the order of 20 μm in diameter and the pellets have dimensions on the order of millimeters. Mate's Sr ferrite magnetic compounds yield bonded magnets significantly weaker than those made of Mate's SmCo and NdFeB compounds. Moreover, Mate's SmCo compounds are anisotropic, i.e., they have a preferential direction of magnetization; because of that, a strong external electromagnetic field needs to be applied during the formation of the bonded magnet to orient the magnetic powder. Therefore, FFF printing SmCo compound would yield permanent magnets with significantly less magnetization. In contrast, Mate's NdFeB magnetic compounds are isotropic, i.e., they magnetize the same regardless of the orientation of the magnetic microparticles embedded in the polymer matrix. We chose Nylon 12 as binder because (i) we already had developed a reliable process to print Nylon 12 via FFF [27], (ii) the structural parts of the actuators could be made of Nylon 12 because of its excellent mechanical properties, and (iii) given that FFF-printed Nylon 12 only sticks well to itself, using Nylon 12 for both the magnetic material and the structural material would greatly facilitate the monolithic manufacture of the bi-material actuators.

For an actuator application it is highly desirable to use feedstock with the highest remanence and energy product that could be extruded into an FFF-printable filament. A range of isotropic materials made of un-magnetized NdFeB microparticles embedded in high per-volume concentrations in Nylon 12 was explored; in particular, the compound RNI-80HR1 (B_r equal to 627 mT, mass density equal to 5.54 g/cm^3, 69% NdFeB by volume –the upper bound of the range tested) and the compound RNI-40LF (B_r equal to 437 mT, mass density equal to 4.49 g/cm^3, 55% NdFeB by volume –the lower bound of the range tested). A Filabot EX2 extruder (Filabot Corporation, Barre VT, USA) was employed to create the printable magnetic filament; the EX2 has a hopper where pellet feedstock is introduced and fed to a three-stage extrusion screw made of hardened and polished high-carbon stainless steel that melts and mixes the pellets, to eventually feed material to a hot nozzle that can reach temperatures as high as 400 °C. The mixing capability of the screw is enhanced by the utilization of a progressive compression section that applies shear force between the polymer and the barrel wall. The screw of the EX2 has a speed control that regulates its rotational speed, compensating for the time-varying forces during the extrusion process [34]. A filament spooler (Filabot

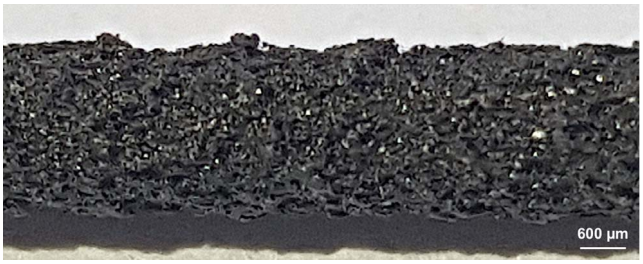

Fig. 2. Close-up optical image of an extruded magnetic filament using pellets made of the compound RNI-40LF. The rough, scaled surface is an artifact of the extrusion process for such a heavily doped material.

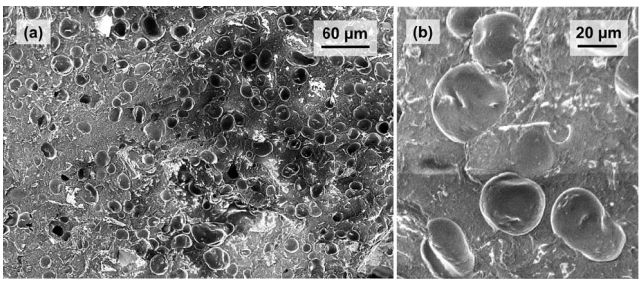

Fig. 3. Micrograph of a cross-section of an extruded magnetic filament made from pellets of the compound RNI-40LF (a) and close-up of the magnetic microparticles embedded in the polymer matrix (b). From metrology of micrographs, the average size of the spheroidal particles is estimated at 18.60 μm $\pm$ 6.29 μm.

Corporation, Barre VT, USA) is placed in front of the nozzle of the extruder to catch the warm filament as it is manufactured and collected with a reel. The Filabot Spooler finely tunes the diameter of the filament by adjusting the speed of the puller wheels that draw the filament from the extruder spout. The puller wheels are non-compressive to preserve the quality of the extrusion [35]. Using the extruder and the spooler typically results in filament diameter tolerances of $\pm$ 0.05 mm [34]. Prior to extrusion, the pellet feedstock was baked in nitrogen at a temperature of 77 °C for 3 days to drive off moisture. Extrusion of the pellet material at 160 °C or at a lower temperature was not feasible. At a slightly higher extrusion temperature (170 °C), a filament can be extruded, but the filament is brittle and would not spool; this temperature is lower than the melting temperature of pure Nylon 12 ($\sim$180 °C) –we speculate this is due to the high concentration of magnetic particles within the polymer. At 180 °C, the extruded filament would break under its own weight. Both pellet materials yielded filaments at an extrusion temperature setting of 170 °C, although with rough, scaled surfaces (Figure 2) –also arguably because of the high concentration of microparticles in the composite; however, the filament made with RNI-80HR1 did not hold together after extrusion. The filament made of the RNI-40LF did hold together, and straight, 70 mm-long strands were produced with an average diameter of 2.5 mm, i.e., slightly thinner than the 2.85 mm standard size of FFF-printable filaments. While the filament was still warm, a 5 m-long filament was also wound onto a spool; however, after cooling, the filament is brittle, snapping when flexed beyond an angle of about 40°. Consequently, the home-built magnetic filament cannot be fed into the printer head in the traditional manner, i.e., by pulling a filament wound onto a spool through a set of feeding gears into an arched tube 180° to the hot nozzle for extrusion. Instead, a specialized method to feed the magnetic filament was devised (see Section II.C).

Sections of the magnetic filaments were characterized using a Zeiss Merlin high resolution SEM (Carl Zeiss Microscopy, Jena, Germany). The magnetic microparticles visible in the images are spheroidal and come in a range of sizes (Figure 3). In general, good spread of the particles across the polymer matrix was observed. The size distribution of the particles was estimated using first Adobe Photoshop software (Adobe, San Jose CA, USA) to outline the beads and then software ImageJ (National Institute of Mental Health, Bethesda MD, USA) to estimate the size of each microbead from the pixels it occupies. The microparticles imaged in the SEM micrographs are not exactly spherical; however, by approximating circular cross-sections, the effective diameters were calculated. The average diameter of the magnetic microparticles from a 393-microparticle set randomly taken is estimated at 18.60 μm $\pm$ 6.29 μm, i.e., below 1% of the diameter of the filament.

The surface roughness, Young's modulus, and hardness of hard-magnetic filament samples were characterized. The roughness of the filament was measured with a confocal microscope (Mitutoyo Quick Vision ACTIVE 202, Mitutoyo America Corporation, Marlborough MA, USA) using the standards ISO 4287 [36] and 4288 [37]; the arithmetic average surface roughness, S_a, is estimated at 58.55 μm. The Young's modulus of the filament was measured via three-point bending tests of straight, 50 mm-long samples with a Pasco Materials Testing System ME-8230 (Pasco, Roseville CA, USA) using the Bending Accessory (ME-8237) at a uniform bending rate of 2.78 mm/min and a sampling rate of 5 Hz. The average Young's modulus is estimated at 3.59 GPa, which is almost six times larger than the Young's modulus of pure Nylon 12 experimentally found for FFF-printed samples (606 MPa [27]) –likely due to the large concentration of NdFeB microparticles within the polymer. The hardness of the filament was measured with a Shore D durometer (560-10D Digital Hardness Meter, Gain Express, Kowloon, Hong Kong) calibrated with standards (64AAA590, Mitutoyo America Corporation, Marlborough MA, USA); the average Shore D harness is estimated at 71.5 –similar to the hardness of high-density polyethylene.

The process used in this study to optimize the formulation of the hard-magnetic filament was inherently empirical, looking to produce filaments of the highest volume concentration of magnetic filler. Mate Corporation supplies NdFeB magnetic compound with filler volume fraction between 55% and 77%. The only magnetic compound that yielded FFF-printable filaments in this study corresponds to the formulation with the smallest volume fraction manufactured by the vendor. We tried magnetic compounds with over 55% volume concentration, but we were unable to produce filaments that would not break immediately after coming out of the extruder. However,

it might be possible to extrude hard-magnetic filaments made of Nylon 12 with over 55% volume concentration of NdFeB microparticles. It might also be possible to use a different polymer, or a different magnetic powder to attain a stronger magnet. A possibility not investigated in this study is the use of anisotropic magnetic compound formulations and the modification of the 3D printer to be able to apply an external electromagnetic field to orient the microparticles during the formation of the magnetic parts. Finally, it might be possible to fabricate flexible filaments by reducing the volume concentration of the filler via the addition of pure polymer pellets to the extrusion mix, although this approach would result in bonded magnets with weaker magnetic properties.

C. Feature Resolution of the Printed Magnetic Material

Step pyramids were printed with filament made of the RNI-40LF composite using 150 μm-thick layers; metrology of the structures was conducted with a calibrated micrometer model 293-832-30 (Mitutoyo, Kanagawa, Japan) to assess the fidelity of the dimensions of the prints compared to the CAD files. In these experiments, the X- and Y-directions correspond to the in-plane dimensions, while the Z-direction corresponds to the out-of-plane dimension; the in-plane dimensions are multiples of the printed traces, which are, in general, equal to the nozzle diameter [38]. Metrology of the structures shows linearity and good correspondence between the measurements of the printed objects and the corresponding dimensions in the CAD files (Figure 4). The offset in the Z-direction of the objects is about 30 μm –a small fraction of a layer, but larger than the offset of a few microns found in analogous structures made of pure Nylon 12 via FFF [27]. The larger Z-offset of the magnetic prints might be due to magnetic beads profusely percolating to the surface of the printed parts upon cooling; this way, the particles would decorate the surface, adding height to the top layer and this would account for the 30 μm offset. The offset in the X- and Y-directions of the printed magnetic composite parts are around 1 mm, i.e., about 3 times larger than the measured offsets of similar parts printed in pure Nylon 12 [27]. The extra width of the magnetic prints compared with the pure-Nylon prints is likely due to the specifications of the recipe used to print the magnetic filament. Through trial and error, it was determined that to attain void-free magnetic composite parts, the filament had to be fed at a higher rate than that used with the pure Nylon 12 filament, leading to excess material around the edges of the parts. However, to the X- and Y-offsets are repeatable, hence can be compensated for when generating the gcode file used to run the printing job.

The dimensional range of features that can be printed via FFF are limited, in practice, by the printing hardware:

- The largest features that could be created are limited by the printing volume of the specific printer; the CreatBot DX Plus used in this study can make objects as large as 250 mm (∼10 inch) by 300 mm (∼12 inch) by 520 mm (20.5 inches) in X, Y, and Z, respectively.
- The smallest in-plane (XY) features that can be made are controlled by the width of the traces, which to first order is equal to the diameter of the nozzle. In FFF printing, the external part of each layer is created using one or more closed loops (called *walls*); it is possible to have significant overlapping between adjacent traces. The narrowest features are composed of only one closed loop (i.e., no infill). The smallest features that we could make with the 600 μm-diameter nozzle were 750 μm wide (a single closed-loop with 75% overlap) when the printed structure is significantly larger in the other in-plane direction [38]; for symmetric features, the smallest dimension we could print is equal to 4 mm. It is possible to use a nozzle with smaller diameter to print the magnetic material, although likely not smaller than 400 μm because the nozzle would then be prone to clogging while extruding composite feedstock [38].
- The smallest vertical feature (Z) that can be created is equal to the height of the printed layers. We have been successful at printing down to 75 μm-tall layers. When creating the CAD file, all vertical features should be a multiple of the layer height.

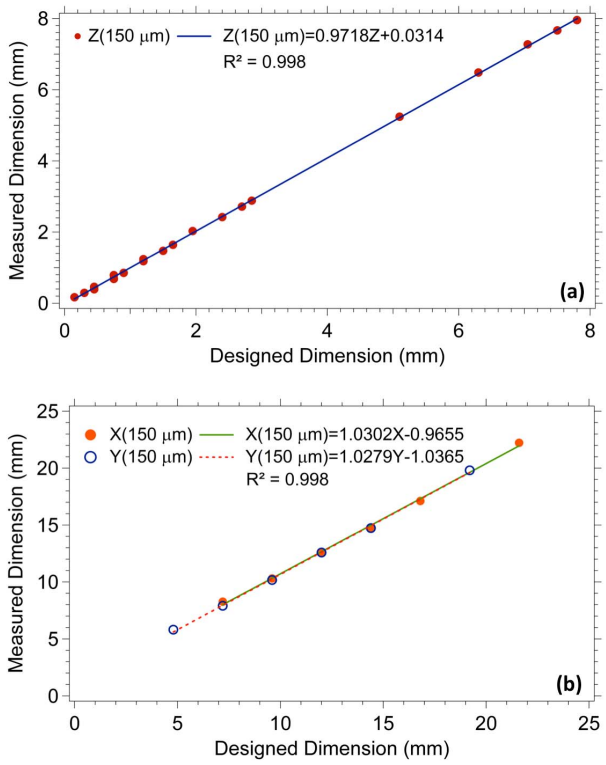

Fig. 4. Measured dimension versus corresponding CAD dimension for the (a) out-of-plane dimensions of the objects and (b) in-plane dimensions of the objects. Linearity and close correspondence between the printed and CAD dimensions are observed.

Any feature above the minimum size in XY and Z is resolved with high accuracy, as shown in Figure 4. The XY and Z positioning precision of the printer are 12.7 μm and 1.25 μm, respectively (from the printer's manufacturer). The magnetic particles are on the order of 20 μm in size, they can stick out of the printed layer, which creates some topography/deviation from the CAD model.

A specialized printing procedure was devised to handle the brittle magnetic filaments, as they are prone to break if they

Fig. 5. An example of a finely FFF-printed magnet using filament made of pellets of the compound RNI-40LF. Individual 150 μm-thick layers are visible on the side of the printed object, as well as 600 μm-wide strips on its top.

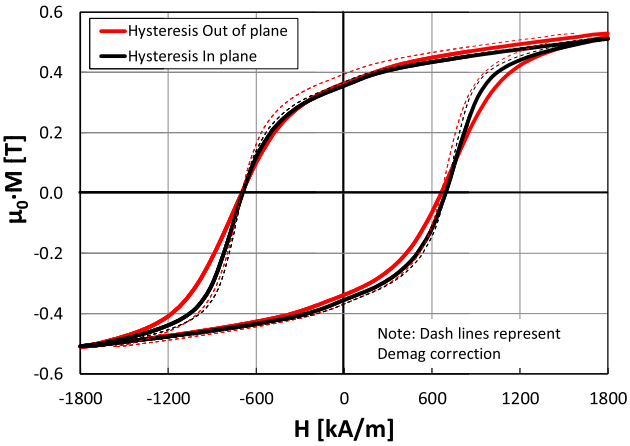

Fig. 6. In-plane and out-of-plane magnetization curves for finely FFF-printed sample made of the compound RNI-40LF.

are bent beyond about 40°. The printer we used in this study is of the Bowden type. Specifically, it has three 70-mm long plastic tubes arched between the filament feeders on the back plane of the printer (stepper motors with gear teeth) and the print head with the three extrusion nozzles suspended above the print bed. Besides issues with the length of the strands of filament we had available and the fragility of the filament, the rough surface of the magnetic filament was found to greatly hamper the capability of the gear teeth to precisely control the filament feed, e.g., effectively do retraction, resulting in the loss of ability to satisfactorily control the material flow rate. Therefore, to overcome these issues, printing of the magnetic filament is accomplished by loading a pure Nylon filament through the fiber feeder and out the disconnected end of the flexible tube at the print head; a piece of magnetic straight filament is joined with fiber-glass reinforced tape to the end of the Nylon filament, and then pushed into the tube. The tube is reconnected to the hot end, setting the printer ready for operation. This configuration allows for the precise control of the magnetic material delivery rate during printing by controlling the feed rate of the pure Nylon 12 filament. An example of a magnet printed by this technique and exhibiting the fine level of dimensional control is shown in Figure 5.

D. Mechanical Properties and Surface Roughness of the Printed Magnetic Material

The surface roughness, Young's modulus, and yield strength of FFF-printed samples made of hard-magnetic filament were characterized. The roughness of the printed objects on the direction parallel to the printed layers was measured with a confocal microscope (Mitutoyo Quick Vision ACTIVE 202, Mitutoyo America Corporation, Marlborough MA, USA) using the standards ISO 4287 [36] and 4288 [37]; the arithmetic average surface roughness, S_a, is estimated at 5.79 μm, which is an order of magnitude smaller than the roughness of the hard-magnetic filament and about four times the reported roughness values from FFF-printed parts made of pure polymers, e.g., PLA [38]. The Young's modulus and yield strength of FFF-printed hard-magnetic samples were measured via compression tests of 8.50 mm long, 8.50 mm wide, and 6.00 mm tall samples with a Pasco Materials Testing System ME-8230 (Pasco, Roseville CA, USA) using the Compression Accessory (ME-8247) at a uniform compression rate of 2.78 mm/min and a sampling rate of 5 Hz. The average Young's modulus is estimated at 2.02 GPa, which is over three times larger than the Young's modulus of pure Nylon 12 experimentally found for FFF-printed samples (606 MPa [27]); we hypothesize this is due to the large concentration of NdFeB microparticles within the polymer matrix. The reduction in Young's modulus compared to the filament value suggests that the reflow of the magnetic material during printing causes softening. The average yield strength of the FFF-printed hard-magnetic filament is estimated at 55.99 MPa $\pm$ 4.59 MPa, which is about twice the yield strength of FFF-printed pure Nylon 12 estimated from uniaxial tests (37.9 $\pm$ 3.5 MPa [27]).

E. Magnetic Properties of the Printed Magnetic Material

For the purpose of magnetic characterization, a finely FFF-printed sample made of the hard-magnetic filament composed of pellets of the compound RNI-40LF was manually machined and polished into a rectangular cuboidal shape with volume equal to about 35.4 mm^3. No chemical modification was performed before measurement. Pulsed magnetization in the Z-axis direction at $\sim$7 T was performed using a Magnetizer 340 B (Oersted Technology, Sandy OR, USA) before measurement. The magnetic properties were calculated based on the measurement of the moment versus applied field (M-H) loops, using a vibrating sample magnetometer EV9 (KLA-Tencor Corporation ADE Division, Westwood MA, USA). M versus H hysteresis loops from the material (Figure 6) were measured at room temperature in the out-of-plane direction (i.e., perpendicular to the printed layers) and in an in-plane direction (i.e., parallel to the printed layers). The material showed a clear hard ferromagnetic response; in addition, no significant variation is perceived between the measurements in both directions, suggesting that the magnetic properties

TABLE I
MAGNETIC PROPERTIES OF FFF-PRINTED SAMPLE MADE OF PELLETS OF THE COMPOUND RNI-40LF

	Orientation	H_c [kA/m]	H_{ci} [kA/m]	Br [mT]	BH_{max} [kJ/m^3]
Vendor specifications	Isotropic	302	756	437	33
Measured	Out of Plane	270	699	395	27
	In Plane	252	692	368	23

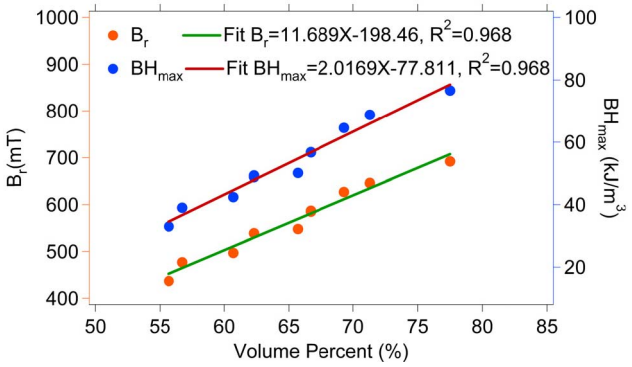

Fig. 7. Magnetic remanence and maximum energy product for Mate Corporation's NdFeB-filled Nylon 12 magnetic compound.

of the material are isotropic. The coercivity (H_c), intrinsic coercivity (H_{ci}), remanence (B_r), and in-plane and out-of-plane energy product of the sample (BH_{max}) are summarized in Table 1. Measured values after FFF-printing are compared with vendor specifications of the raw material. The maximum observable change in properties was a reduction of 30% in the energy product, which is attributed to a decrease in remanence –most likely due to changes in density in the material during the fusing process. Nonetheless, the printed magnets have stronger magnetic remanence by nearly 30% and higher density by up to 18% compared to FFF-printed hard magnets previously reported by other research groups [24], [25].

Figure 7 shows the magnetic remanence and maximum energy product versus volume fraction for Mate's NdFeB magnetic compound; the volume fraction spans the 55% to 77% range. The remanence monotonically increases between 437 mT and 692 mT, while the maximum energy product monotonically increases between 33 KJ/m^3 and 77 KJ/m^3; in both cases, a linear least-squares fitting adequately describes the functional dependence between the magnetic property and the volume fraction of magnetic filler; however, the relationship does not reflect a simple rule of mixtures (e.g., the least-square fittings don't pass through zero). Although there is a direct correlation between remanence and ferromagnetic particle volume fraction, to the extent of the authors' acknowledge there is no comprehensive analysis between hard magnetic material behavior and composite formation. Mixing rules and theoretical analysis for ferromagnetic composites exist, but the body of research focuses on characterizing the magnetic permeability at high frequencies [39] and in soft ferromagnets [40].

In our approach, the printed parts are magnetized after printing, which could limit the kind of structures that can be realized. However, post-printing magnetization is compatible with a standard FFF printer, greatly facilitating the replication of our work by other researchers. Moreover, post-fabrication magnetization is the standard procedure in commercial magnets and most MEMS magnets are post-fabricated magnetized, e.g., using pulse magnetization; post-fabrication magnetization not only aligns the internal magnetic domains that get disoriented due to thermal and mechanical stresses induced at fabrication (and internal flow of particulate material in liquid state polymer during extrusion), but guaranties the maximum energy product of the given magnet by fully saturating the material [20]. In addition, it might be possible to use a second material in a dual-extruder FFF printer to create a support structure to successfully accomplish the post-printing magnetization of a freeform object; the support material would then be removed. Using a support material is commonly used to print intricate objects via FFF [41]; we hypothesize that polymers such as acrylonitrile (ABS), high-impact polystyrene (HIPS) or polyvinyl alcohol (PVA) could be used to play such role for parts made in Nylon 12 (ABS is dissolved by acetone, HIPS is dissolved by d-limonene, and PVA is dissolved by water, while Nylon 12 is not affected by any of these chemicals).

F. Magnetic Field Finite Element Simulations

The stray magnetic field produced by an FFF-printed sample (after pulsed magnetization) was modeled using version 5.3a of COMSOL Multiphysics (COMSOL, Inc., Burlington MA, USA). The finite-element method is used to solve the magneto-quasistatic Maxwell equations, following the methods reported in [42]. The second quadrant of the experimentally measured nonlinear magnetic properties of the Nylon 12/NdFeB compound RNI-40LF (see Section II.E) were used in the simulations. For this study, a structure composed of a cylindrical magnet with outer diameter and height equal to 12.75 mm and 7.68 mm, respectively, attached to a 150 μm-thick membrane was chosen and fabricated. A 2D axisymmetric model of a FFF-printed magnet was simulated; a 3D representation of the stray magnetic field (revolution of the 2D axisymmetric plot) is presented in Figure 8. From the simulation results, sub-Tesla fields are expected in the space near the horizontal free surface of the printed magnet.

To validate the simulations and characterize the magnetic behavior of the FFF-printed object, the intensity of the stray magnetic field in the axial line above the magnet (B_z) was measured by using an in-house designed and fabricated scanning Hall probe (SHP). A comparison between measurements and simulations is presented in Figure 9; good agreement between the finite element results and measurements is found. According to the simulations, the maximum field at the surface of the magnet is ~147 mT and the magnetic field at 14 mm from the surface decays below 95% of the maximum field.

III. DEVICE DESIGN AND FABRICATION

The proof-of-concept, monolithic, bi-material magnetic actuator design is a cylindrical frame made in Nylon 12,

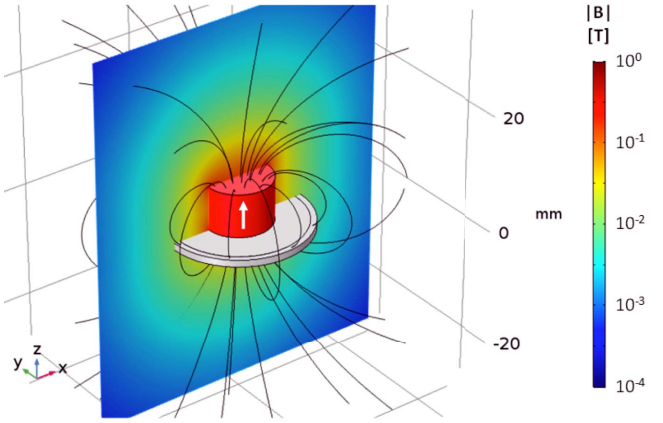

Fig. 8. 3D representation of the stray magnetic field produced by a printed magnet made of Nylon 12/NdFeB compound RNI-40LF. In the figure, the black lines represent the B field, and the white arrow represents the direction of the magnetization (M_z) inside the magnet.

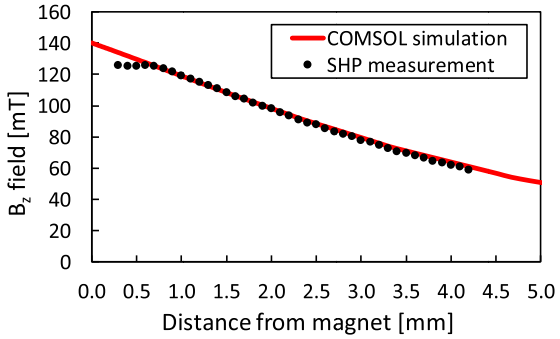

Fig. 9. Magnetic flux density in the Z-direction (B_Z) as a function of the distance from the surface of the magnet: scanning Hall measurements (black dotted line) and finite element simulation results (red continuous line).

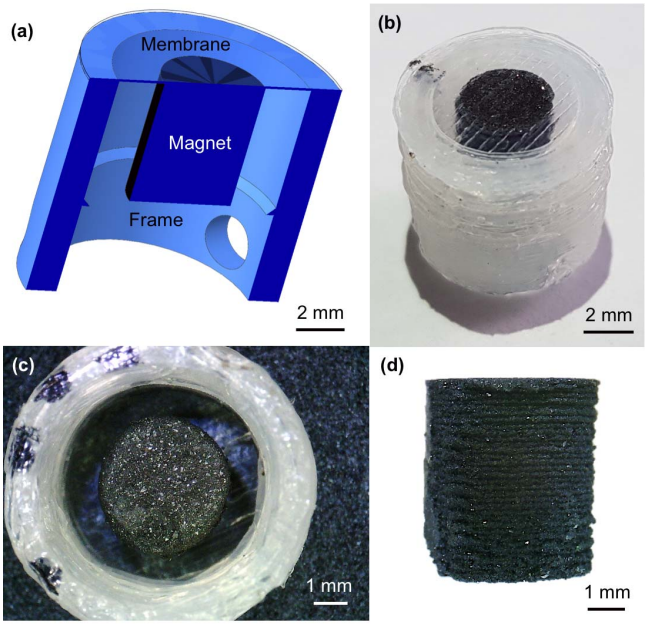

Fig. 10. A collection of images of an FFF-printed mini magnetic actuator including (a) a CAD cross-section, (b) top view of a printed actuator, (c) bottom view of the device, and (d) side view of a printed magnet removed from an actuator.

fused to a flat membrane made of Nylon 12, which in turn is attached at its center to a magnet made of the Nylon 12/NdFeB compound RNI-40LF (Figure 10). The printed magnets are made of NdFeB magnetic compound with the highest volume concentration we identified that yielded extruded filaments and FFF-printed objects (i.e., 55%). The binder of the magnetic material is the same material used in the structural components of the actuator, resulting in good adhesion between the magnetic and structural parts of the actuator. The actuator design was synthesized without a specific application in mind; however, the actuator and its bonded magnet are compatible with a wide range of temperatures, including near-room temperature operation. The actual dimensions of the different components of the device resulted from iteration of the design and optimization of the printing recipes, looking to synthesize the smallest possible actuators with associated repeatable fabrication. There are practical limits regarding how thin a membrane or how small a structure can be FFF-printed reliably for a given printer, feedstock, and nozzle diameter. Using 600 μm-diameter nozzles (600 μm nominal trace width), the thinnest single-layer Nylon 12 membranes that were repeatable, robust, and leak tight had a nominal thickness equal to 100 μm. In addition, using 600 μm-diameter nozzles, the thinnest hard-magnetic layers that could be repeatably printed were as thin as 75 μm; using narrower nozzles would likely result in clogging due to the large concentration of microparticles embedded in the polymer matrix. Although cylindrical frames with single-shell thickness equal to 600 μm, 6 mm outer diameter, and 7 mm height could be printed in Nylon 12, they would easily break apart when manipulated, e.g., while setting them up for testing. The thinnest wall frame made in Nylon 12 that could be repeatably printed is a two-shell structure with 1.2 mm thickness, 10 mm outer diameter, and 9 mm height. The smallest diameter of the magnets that could be reliably printed was found equal to 4 mm.

To print the magnetic actuator, the printer bed is heated at 60 °C and then coated with a thin layer of PVAc adhesive. After that, the temperature of the bed is raised to 80 °C and Nylon 12 priming pads are printed onto the adhesive film to ensure the nozzle is producing a steady flow of melted thermoplastic. Then, a 24 mm-diameter Nylon 12 membrane is printed. On top of the membrane, the foundation of a 10 mm diameter, 1.2 mm-thick wall is printed, centered on the 24 mm-diameter membrane; this is followed by printing the first layer of a Nylon 12 priming pillar, located 20 mm from the center of the frame foundation (Figure 11 (a)). Most FFF printers run their nozzle(s) in open loop, i.e., the printer assumes material is coming out of the active nozzle while rastering the layer that is meant to be printed. In general, in a single-material print there are no issues with this approach, but when using two or more filaments, it is important to make sure that the active nozzle is steadily ejecting material; this is achieved by printing dummy structures before printing the actual device structures. Consequently, the fabrication process continues by printing priming pads of the magnetic material, followed by the first layer of a magnetic material

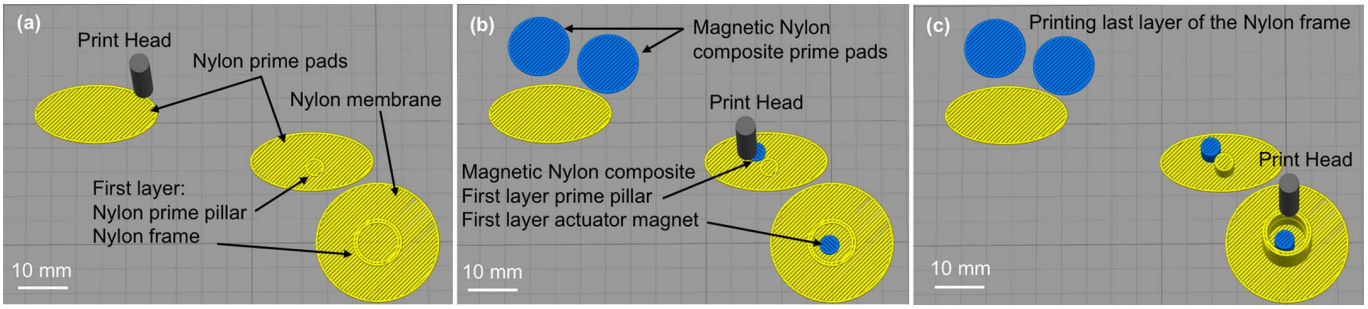

Fig. 11. Intermediate steps in a Simplify3D simulation of the multi-material FFF printing process used to create the monolithic magnetic actuators: (a) stabilizing the Nylon 12 flow rate by printing prime pads (24 mm diameter membrane), printing the first layer of a Nylon frame on top of the membrane, and printing a 4 mm diameter priming pillar on top of the priming pad; (b) stabilizing the flow rate of the magnetic composite material and printing the first magnet layer and magnet priming pillar layer in a similar manner to that used for the pure Nylon 12; (c) printing the final layer of Nylon 12 to complete the device.

priming pillar and then the first layer of the magnet centered in the actuator frame (Figure 11 (b)). Going forward in the process, the Nylon 12 priming pillar n^{th} layer is printed first and in front of the magnetic material priming pillar; in this manner, the Nylon 12 priming pillar acts as a wiping post for the magnetic material, which greatly reduces the amount of spurious magnetic material incorporated into the Nylon frame (Figure 11 (c)). An example of magnetic material inclusion into a Nylon actuator frame is visible in Figure 10 (b), where the black magnetic material is incorporated into the clear Nylon 12 frame in the upper left quadrant of the part; this unwanted deposition took place when the hot nozzle containing the molten magnetic composite thermoplastic traveled across the outer wall of the actuator on its path to print a magnetic layer inside the actuator.

Compensation to global X- and Y-offsets was introduced in the software that generated the gcode file to account for the misalignment of the two nozzles; the correction is evident in Figure 11 (b) and (c), where the blue magnet is off-center inside the yellow Nylon 12 frame; nonetheless, the actual printed object is properly aligned.

The magnetic composites are printed in an un-magnetized state –the processing temperature (250 °C) is far greater than the Curie temperature of NdFeB ceramic magnets (80 °C). Post printing, the actuators were inserted between the poles of an electromagnet with the major axis of the magnet parallel to the magnetic field lines; field strength was slowly increased from 0 T up to 1.4 T and back down, and then the actuator was removed with the printed RNI-40LF in a fully magnetized state.

IV. Structural Finite Element Analysis of Actuator

3D finite element simulations of the mechanical performance of the actuator design were conducted using SolidWorks 2015 (Dassault Systèmes, Waltham MA, USA). In these simulations, the parts made of Nylon 12 had a Young's modulus, Poisson ratio, and mass density equal to 606 MPa [27], 0.35 [43], and 1.01 g/cm^3 [44], respectively. The parts made of the composite RNI-40LF had a Young's modulus and Poisson ratio equal to 2.02 GPa and 0.35, respectively (the latter assumed to be equal to the corresponding value for pure Nylon 12); the density of the printed magnets was estimated by measuring the dimensions and weights of test structures and taking the ratio between their mass and volume –a value of 3.79 g/cm^3 was calculated, which is significantly smaller than the value of 4.49 g/cm^3 provided by the vendor of the unprocessed pellets.

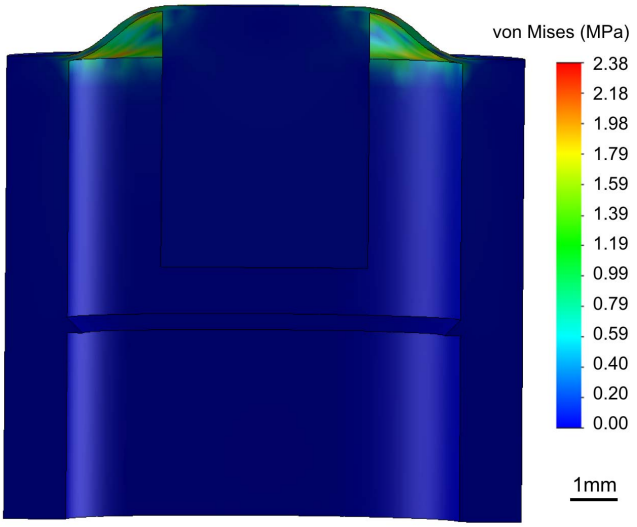

Fig. 12. Static finite element analysis of the actuator with a 0.352 N force applied to the face of the magnet in the Z direction; the resulting displacement in the Z direction is 50 μm, and the maximum stress on the membrane is 2.38 MPa.

The finite element simulations of the static deflection of the membrane due to an on-axis central force applied to the magnet component predict that a force of 0.352 N on the magnet results in a 50 μm maximum membrane displacement, while causing a maximum stress equal to 2.38 MPa (Figure 12), i.e., well below the limit for fatigue infinite life of Nylon 12 ($\sim$19 MPa [45]) or the yield strength of FFF-printed Nylon 12 (37.9 $\pm$ 3.5 MPa –estimated from uniaxial tests of printed parts [27]). The displacement is small enough compared to the thickness of the membrane to not trigger non-linear elastic effects [46].

The resonance modes of the actuator were also simulated using SolidWorks 2015 (Figure 13). The first two orthog-

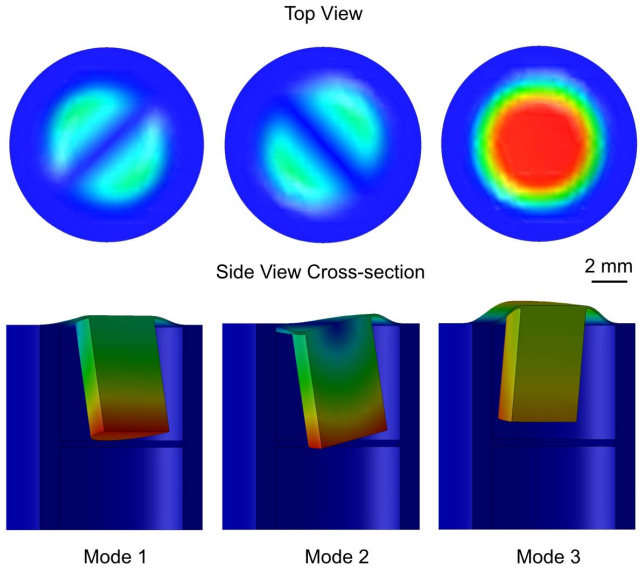

Fig. 13. Simulation results for the first 3 modes of vibration of the actuator. Modes 1 and 2 are orthogonal and occur at frequencies equal to 592.61 Hz and 597.4 Hz, respectively. Mode 3, at a frequency of 875.98 Hz, results in an up and down displacement of the center of the membrane in the Z-direction.

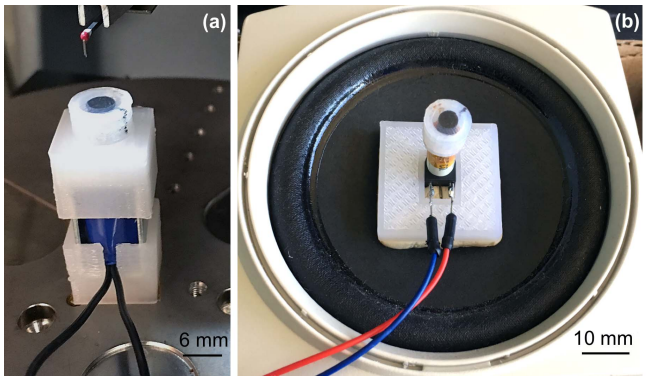

Fig. 14. Experimental set up to measure radial membrane displacement under an applied force (a) and to measure resonance modes under an applied harmonic displacement (b).

onal vibration modes are closely spaced at 592.61 Hz and 597.43 Hz, in which the magnet swings back and forth in the X-direction (mode 1) or the Y-direction (mode 2), creating a two-lobed displacement in the Z-direction on the membrane surface (Figure 13, left and center). There is a third resonance mode at 875.98 Hz, in which a single-lobed displacement in the Z-direction of the membrane is generated, while a back and forth motion in both the X- and Y-directions of the magnet takes place (Figure 13, right).

V. Experimental Results and Discussion

The radial displacement of an FFF-printed magnetic actuator was characterized with a Dektak stylus profilometer (Bruker, Tucson AZ, USA) with ± 500 μm vertical range (Figure 14 (a)). The actuator was mounted on top of a spring-loaded mini-solenoid (Adafruit part 2776) with a stroke equal to 3 mm and 0.78 N force at 5 V DC; the magnet is in contact

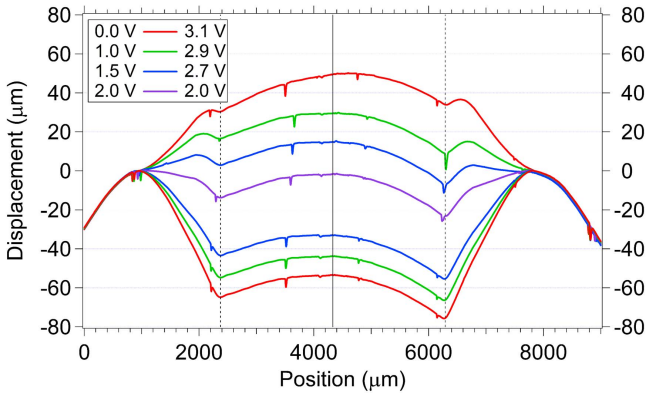

Fig. 15. Membrane displacement versus radial position (zero is at edge of the membrane) for various loads for a magnetic actuator with a 100 μm-thick membrane; ± 50 μm displacement was measured. The 5 to 10 μm deep notches in a few of the traces are the actual seams between the printed strips of Nylon 12 comprising the membrane surface, which is similar to the reported topography of FFF-printed in-plane surfaces [37].

with the iron armature of the solenoid and displaces it by about half the stroke (1.7 mm) when mounted (this compresses the spring on the armature and provides a force on the membrane). Due to the spring force, a displacement of 50 μm is measured with no voltage applied (Figure 15). When voltage is applied to the coil, it pulls the membrane down from equilibrium; at about 2 V DC the membrane is near zero displacement, and near 3.1 V DC the membrane is displaced by -50 μm. The shape of the displaced membrane is approximately symmetric and has a similar profile to the simulated membrane under a force in Figure 12. Armature decoupling from the printed magnet occurs at a voltage of about 3.3 V DC.

In order to measure its resonant properties, the miniature magnetic actuator was mounted on top of a coil held in place by a 3D-printed Nylon 12 base affixed with putty to a mid-range audio transducer (Figure 14 (b)). The coil was removed from a reed relay (RSR Electronics, Rahway NJ, USA, part 22RD5, 5 V DC, 500 Ω, 7 mm outer diameter) and Kapton tape was applied to the end to prevent the coil from unwinding. The mini magnetic actuator was mounted on top with the magnet suspended by a distance of approximately 300 μm from the coil. For an input signal, sinusoidal waves of varying frequency produced by a waveform generator Wavestation model 2052 (Teledyne LeCroy, Chestnut Ridge NY, USA) were sent to an audio frequency amplifier connected to the audio transducer. The output voltage of the coil was measured with an oscilloscope Rigol model DS6000 (Rigol USA, Beaverton OR, USA). Simulation results predict the first three resonance frequency modes of the magnetic actuator at 592.61 Hz, 597.43 Hz, and 875.98 Hz (see Section IV); consequently, the frequency of the sine waves produced by the waveform generator was varied manually in 10 Hz steps between 500 Hz and 3 kHz to capture the resonances, and in 100 Hz steps in lower and higher frequency ranges. A plot of peak-to-peak coil output voltage versus frequency is displayed in Figure 16 –a background noise level of 131 mV is subtracted from the readings. The signal is quite strong with a pronounced peak at 610 Hz, within 3% of the first two simulated vibration modes (red bars in Figure 16). At frequencies

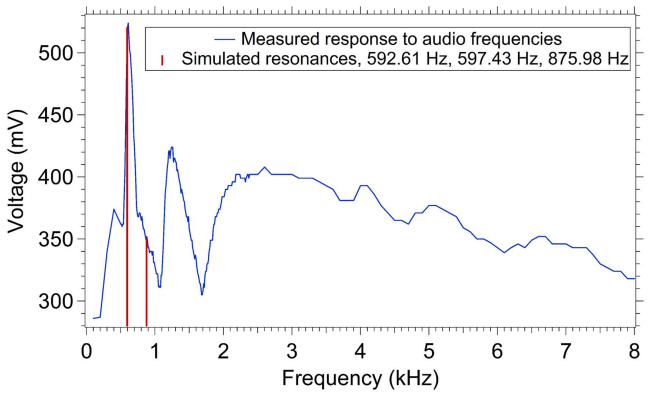

Fig. 16. Peak-to-peak pick-up coil output voltage versus displacement frequency input to an audio transducer (blue). A pronounced resonance peak is recorded at a frequency of 610 Hz, which correlates well with the results of finite element simulations of the first two modes of vibration of the mini-actuator (red –see Section IV). Other features are most likely associated with vibration modes of other components of the experimental setup and not the mini actuator itself.

lower than 600 Hz and higher than 1 kHz, there are several lower amplitude features compared with the strong feature at 610 Hz that should represent other vibration modes –most likely not associated with the miniature magnetic actuator itself, but rather with other components of the experimental setup.

3D printing cannot compete in cost with other manufacturing methods in large-volume production of parts with the same geometry; however, multiple studies have shown that additive manufacturing is the cheaper approach when producing low-volume batches, complex parts, and customized parts [47], [48]. The maximum number of parts that are cheaper to make via additive manufacturing vs. a traditional method depends on factors such as the geometry of the part, dimensions, materials, etc., but it roughly oscillates between tens of units and tens of thousands of units [49].

The actuators reported in this study are arguably complex: they are small, monolithically made of two distinctive materials, with finely featured components and gaps; precise assembly of their components is needed to attain good symmetry and actuate properly. Making each of these actuators takes 0.35 grams of Nylon 12 and 0.35 grams of RNI-40LF, for a total cost in materials equal to $1.01 ($0.03 for the Nylon 12 and $0.98 for the magnetic compound). The printer used in this study costs under $2,000 and can process a wide variety of customized designs, including last-minute variations, at no extra expense; this cost compares favorably with that of a typical apparatus to form bonded magnets (e.g., each injection mold would cost at least $1,500 [50]).

VI. Conclusion

We reported the design, fabrication, and characterization of the first monolithically 3D-printed, multi-material compact magnetic actuators in the literature; the devices incorporate a hard magnet made of a composite of NdFeB microparticles embedded in Nylon 12 (55% by volume) and a leak-tight membrane and structural components made of pure Nylon 12. The miniature actuator, 3D-printed via FFF, is composed of a cylindrical frame with 1.2 mm-thick wall that mounts on a solenoid, and a 10 mm diameter, 100 μm-thick membrane connected at its center to a printed hard magnet.

The average surface roughness, Young's modulus, and hardness of the FFF-printable hard-magnetic filament with 55% volume fraction of NdFeB were estimated at 58.55 μm, 3.59 GPa, and Shore D 71.5, respectively, while the average surface roughness, Young's modulus, and yield strength of FFF-printed magnetic material using such filament were estimated at 5.79 μm, 2.02 GPa, and 55.99 MPa $\pm$ 4.59 MPa, respectively.

Magnetic characterization of the FFF-printed magnets demonstrates that the developed fabrication process yields an isotropic hard ferromagnetic material with intrinsic coercivity of $\sim$700 kA/m, remanence of $\sim$395 mT, and maximum energy product of 27 kJ/m^3–outperforming previously reported FFF-printed hard magnets. COMSOL simulations of the stray magnetic field predict a maximum B_z field of 147 mT at the surface of the magnet, decaying by 95% at a distance of 14 mm. A validation of the simulation was performed using measurements with an in-house designed and fabricated scanning Hall probe, showing very good correlation between simulation and experimental data. These results prove that FFF-printed magnets could be used as replacements of assembled magnets in compact systems. The cost in materials for FFF printing one of these actuators is estimated at $1.01, with $0.03 spend in the Nylon 12 components and $0.98 spent in the bonded magnet.

The radial displacement of a single-layer membrane actuator was characterized for various coil bias voltages; a maximum displacement equal to 50 μm was obtained with 3.1 V DC applied to the driving coil. Finite element simulations of the actuator design estimate at 2.38 MPa the maximum stress on the membrane at 50 μm actuation while experiencing a 0.352 N axial force, and at 592.61 Hz the natural frequency of the device. These results demonstrate that is possible to implement compact magnetic actuators via FFF with force and displacement levels of relevance to MEMS.

Acknowledgment

The authors would like to thank Brenda García Farrera, Velásquez-García Research Group, Massachusetts Institute of Technology (Cambridge MA, USA), for helping with SEM micrographs, analysis, and photography of printed structures, Zhumei Sun, Velásquez-García Research Group, Massachusetts Institute of Technology, for helping with the roughness and mechanical properties measurements, Dave Terry, Microsystems Technology Laboratories, Massachusetts Institute of Technology, for his help with the set up to measure audio frequency resonance, the Mate Corporation (Okayama, Japan), for supplying the pellets used to create the FFF-printable filament employed in this study, and Josh Heisler, Filabot Corporation (Barre VT, USA), for helping crafting the magnetic filament used in this study.

References

[1] D. T. Snyder, C. J. Pulliam, Z. Ouyang, and R. G. Cooks, "Miniature and fieldable mass spectrometers: Recent advances," *Anal. Chem.*, vol. 88, no. 1, pp. 2–29, 2015.

[2] R. R. A. Syms and S. Wright, "MEMS mass spectrometers: The next wave of miniaturization," *J. Micromech. Microeng.*, vol. 26, no. 2, 2016, Art. no. 023001.

[3] K. W. Oh and C. H. Ahn, "A review of microvalves," *J. Micromech. Microeng.*, vol. 16, no. 5, pp. R13–R39, 2006.

[4] D. J. Laser and J. G. Santiago, "A review of micropumps," *J. Micromech. Microeng.*, vol. 14, no. 6, pp. R35–R64, 2004.

[5] T. Grzebyk, "MEMS vacuum pumps," *J. Microelectromech. Syst.*, vol. 26, no. 4, pp. 705–717, Aug. 2017.

[6] D. C. Roberts *et al.*, "A piezoelectric microvalve for compact high-frequency, high-differential pressure hydraulic micropumping systems," *J. Microelectromech. Syst.*, vol. 12, no. 1, pp. 81–92, Feb. 2003.

[7] M. M. Sadeghi, H. S. Kim, R. L. B. Peterson, and K. Najafi, "Electrostatic micro-hydraulic systems," *J. Microelectromech. Syst.*, vol. 25, no. 3, pp. 557–569, Jun. 2016.

[8] M. De Volder and D. Reynaerts, "Pneumatic and hydraulic microactuators: A review," *J. Micromech. Microeng.*, vol. 20, no. 4, 2010, Art. no. 043001.

[9] J. Getpreecharsawas, I. Puchades, B. Hournbuckle, L. Fuller, R. Perason, and S. Lyshevshi, "An electromagnetic MEMS actuator for micropumps," in *Proc. 2nd Int. Conf. Perspective Technol. Methods MEMS Des.*, Lviv, Ukraine, May 2006, pp. 11–14.

[10] A. P. Taylor and L. F. Velásquez-García, "Miniaturized diaphragm vacuum pump by multi-material additive manufacturing," *J. Microelectromech. Syst.*, vol. 26, no. 6, pp. 1316–1326, Dec. 2017.

[11] D. I. Wimpenny, P. M. Pandey and J. Kumar, *Advances in 3D Printing & Additive Manufacturing Technologies*. Singapore: Springer, 2017.

[12] D. W. Rosen, "Computer-aided design for additive manufacturing of cellular structures," *Comput. Aided. Des. Appl.*, vol. 4, no. 5, pp. 585–594, 2007.

[13] H. Gong, A. T. Woolley, and G. Nordin, "High density 3D printed microfluidic valves, pumps, and multiplexers," *Lab Chip*, vol. 16, pp. 2450–2458, May 2016.

[14] D. Pranzo, P. Larizza, D. Filippini, and G. Percoco, "Extrusion-based 3D printing of microfluidic devices for chemical and biomedical applications: A topical review," *Micromachines*, vol. 9, no. 8, p. 374, 2018.

[15] E. García-López, D. Olvera-Trejo, and L. F. Velásquez-García, "3D printed multiplexed electrospinning sources for large-scale production of aligned nanofiber mats with small diameter spread," *Nanotechnology*, vol. 28, no. 42, 2017, Art. no. 425302.

[16] D. Olvera-Trejo and L. F. Velásquez-García, "Additively manufactured MEMS multiplexed coaxial electrospray sources for high-throughput, uniform generation of core-shell microparticles," *Lab Chip*, vol. 16, no. 21, pp. 4121–4132, 2016.

[17] E. MacDonald and R. Eicker, "Multiprocess 3D printing for increasing component functionality," *Science*, vol. 353, no. 6307, 2017, Art. no. aaf2093.

[18] K. Gandha *et al.*, "Additive manufacturing of anisotropic hybrid NdFeB-SmFeN nylon composite bonded magnets," *J. Magn. Magn. Mater.*, vol. 467, pp. 8–13, Dec. 2018.

[19] L. Li, B. Post, V. Kunc, A. M. Elliott, and M. P. Paranthaman, "Additive manufacturing of near-net-shape bonded magnets: Prospects and challenges," *Scripta Mater.*, vol. 135, pp. 100–104, Jul. 2017.

[20] D. P. Arnold and N. Wang, "Permanent magnets for MEMS," *J. Microelectromech. Syst.*, vol. 18, no. 6, pp. 1255–1266, Dec. 2009.

[21] Z. Ji, C. Yan, B. Yu, X. Wang, and F. Zhou, "Multimaterials 3D printing for free assembly manufacturing of magnetic driving soft actuator," *Adv. Mater. Inter.*, vol. 4, no. 22, 2017, Art. no. 1700629.

[22] Y. Kim, H. Yuk, R. Zhao, S. A. Chester, and X. Zhao, "Printing ferromagnetic domains for untethered fast-transforming soft materials," *Nature*, vol. 558, pp. 274–279, Jun. 2018.

[23] D. Kokkinis, M. Schaffner, and A. R. Studart, "Multimaterial magnetically assisted 3D printing of composite materials," *Nature Commun.*, vol. 6, p. 8643, Oct. 2015.

[24] C. Huber *et al.*, "3D print of polymer bonded rare-earth magnets, and 3D magnetic field scanning with an end-user 3D printer," *Appl. Phys. Lett.*, vol. 109, no. 16, 2016, Art. no. 162401.

[25] C. Huber *et al.*, "3D printing of polymer-bonded rare-earth magnets with a variable magnetic compound fraction for a predefined stray field," *Sci. Rep.*, vol. 7, p. 9419, Aug. 2017.

[26] B. Khatri, K. Lappe, D. Noetzel, K. Pursche, and T. Hanemann, "A 3D-printable polymer-metal soft-magnetic functional composite—Development and characterization," *Materials*, vol. 11, no. 2, p. 189, 2018.

[27] A. P. Taylor and L. F. Velásquez-García, "High-temperature compatible, monolithic, 3D-printed magnetic actuators," *J. Phys., Conf. Ser.*, vol. 1052, Jul. 2018, Art. no. 012046. doi: 10.1088/1742-6596/1052/1/012046.

[28] *SmCo vs. NdFeB Magnets*. Accessed: Feb. 20, 2019. [Online]. Available: https://www.arnoldmagnetics.com/resources/samarium-cobalt-vs-neodymium-iron-boron/

[29] *Ultra High SmCo Magnets*. Accessed: Feb. 20, 2019. [Online]. Available: https://www.electronenergy.com/ultra-high-temperature-samarium-cobalt-magnets/

[30] D. T. Pham and R. S. Gault, "A comparison of rapid prototyping technologies," *Int. J. Mach. Tools Manuf.*, vol. 38, nos. 10–11, pp. 1257–1287, 1998.

[31] *RoVa3D 5-Extruder 3D Printer*. Accessed: Feb. 20, 2019. [Online]. Available: https://www.ordsolutions.com/rova3d-5-extruder-3d-printer-package/

[32] *Magnetic Iron PLA Filament*. Accessed: Feb. 20, 2019. [Online]. Available: https://www.proto-pasta.com/products/magnetic-iron-pla

[33] *Safety Data Sheet Composite Iron Fiber PLA*. Accessed: Feb. 20, 2019. [Online]. Available: https://www.proto-pasta.com/pages/documentation

[34] *Filabot EX2 Extruder*. Accessed: Feb. 20, 2019. [Online]. Available: https://www.filabot.com/collections/filabot-core/products/filabot-original-ex2

[35] *Filabot Spooler*. Accessed: Feb. 20, 2019. [Online]. Available: https://www.filabot.com/collections/filabot-core/products/filabot-spooler

[36] (1997). *Geometrical Product Specifications (GPS)-Surface Texture: Profile Method-Terms, Definitions and Surface Texture Parameters, ISO 4287*. Accessed: Feb. 20, 2019. [Online]. Available: https://www.iso.org/standard/10132.html

[37] (1996). *Geometrical Product Specifications (GPS)-Surface Texture: Profile Method-Rules and Procedures for the Assessment of Surface Texture, ISO 4288*. Accessed: Feb. 20, 2019. [Online]. Available: https://www.iso.org/standard/2096.html

[38] Z. Sun and L. F. Velásquez-García, "Monolithic FFF-printed, biocompatible, biodegradable, dielectric-conductive microsystems," *J. Microelectromech. Syst.*, vol. 26, no. 6, pp. 1356–1370, Dec. 2017.

[39] A. N. Lagarkov and K. N. Rozanov, "High-frequency behavior of magnetic composites," *J. Magn. Magn. Mater.*, vol. 321, pp. 2082–2092, Jul. 2009.

[40] E. A. Périgo, B. Weidenfeller, P. Kollár, and J. Füzer, "Past, present, and future of soft magnetic composites," *Appl. Phys. Rev.*, vol. 5, no. 3, 2018, Art. no. 031301.

[41] *How to Use Support Material in FFF printing*. Accessed: Feb. 20, 2019. [Online]. Available: https://www.matterhackers.com/news/how-to-use-support-material:-part-2

[42] O. D. Oniku, A. Garraud, E. E. Shorman, W. C. Patterson, and D. P. Arnold, "Modeling of a micromagnetic imprinting process," in *Tech. Dig. Solid-State Sens., Actuators, Microsyst. Workshop (Hilton Head)*, Hilton Head, SC, USA, Jun. 2014, pp. 187–190. doi: 10.31438/trf.hh2014.51.

[43] *Properties Nylon 12*. Accessed: Feb. 20, 2019. [Online]. Available: http://www.matweb.com/search/DataSheet.aspx?MatGUID=0e37a459c4eb452faa9d92659f9a0ccc

[44] W. Griehl and D. Ruestem, "Nylon 12-preparation, properties, and applications," *Ind. Eng. Chem.*, vol. 62, no. 3, pp. 16–22, 1970.

[45] B. Van Hooreweder, D. Moens, R. Boonen, J.-P. Kruth, and P. Sas, "On the difference in material structure and fatigue properties of nylon specimens produced by injection molding and selective laser sintering," *Polym. Test.*, vol. 32, no. 5, pp. 972–981, 2013.

[46] D. C. Roberts, "Design, modeling, fabrication and testing of a piezoelectric microvalve for high pressure, high frequency hydraulic applications," Ph.D. dissertation, Dept. Mech. Eng., Mass. Inst. Technol., Cambridge, MA, USA, 2002.

[47] N. Hopkinson and P. M. Dickens, "Analysis of rapid manufacturing—Using layer manufacturing processes for production," *Proc. Inst. Mech. Eng., Part C, J. Mech. Eng. Sci.*, vol. 217, no. 1, pp. 31–39, 2003.

[48] M. Baumers, "Economic aspects of additive manufacturing: benefits, costs, and energy consumption," M.S. thesis, Dept. Mech., Elect., Manuf. Eng., Loughborough Univ., Loughborough, U.K., 2012.

[49] D. S. Thomas and S. W. Gilbert, "Costs and cost effectiveness of additive manufacturing," *NIST Special Publication*, vol. 1176, Dec. 2014. doi: 10.6028/NIST.SP.1176.

[50] *Plastic Injection Molding*. Accessed: Feb. 20, 2019. [Online]. Available: https://www.protolabs.com/services/injection-molding/plastic-injection-molding/

Anthony P. Taylor received the B.S. degree in physics (*cum laude*) from Saint Lawrence University, Canton, NY, USA, in 1985, the M.S. degree in physics from the University of Arizona, Tucson, AZ, USA, in 1988, and the Ph.D. degree in physics from the Rensselaer Polytechnic Institute, Troy, NY, USA, in 1993.

Until now, he has devoted his career at Edwards Vacuum, Sanborn, NY, USA, as an Applications Engineer and Applications Technologist. He has been a Visiting Scientist with the Velásquez-García Group, Massachusetts Institute of Technology (MIT), since 2014. His work at MIT has been focused on novel fabrication methods of micro and nanosystems, specifically electrospray-printed gas sensors for vacuum and gas abatement applications, and more recently on 3D-printed miniature pumps.

Camilo Vélez Cuervo (S'05–M'12) received the B.S. degree in electronic engineering from Pontificia Universidad Javeriana, Bogotá, Colombia, in 2007, the M.E. degree in electronics and computers from the Universidad de Los Andes, Bogotá, in 2012, and the M.S. degree and the Ph.D. degree in electrical and computer engineering from the University of Florida, Gainesville, FL, USA, in 2015 and 2017, respectively. He is currently a Post-Doctoral Researcher with Carnegie Mellon University. With the experience as a Field Service Engineer at Siemens Healthcare Diagnostics, he has coauthored over 20 refereed journal and conference publications, and he has filed two international patents. His research focuses on micro robotics, micro/nanostructured magnetic materials, MEMS, and microfabrication. He currently serves on the Board of Governors of the IEEE Electron Devices Society (EDS) and as an IEEE EDS Young Professionals Committee Chair.

David P. Arnold (S'97–M'04–SM'10) received the dual B.S. degrees in electrical and computer engineering, in 1999, the M.S. degree in electrical and computer engineering from the University of Florida, Gainesville, FL, USA, in 2001, and the Ph.D. degree in electrical and computer engineering from the Georgia Institute of Technology, Atlanta, GA, USA, in 2004.

He is currently the George Kirkland Engineering Leadership Professor with the Department of Electrical and Computer Engineering, University of Florida, the Deputy Director of the NSF Multi-Functional Integrated System Technology (MIST) Center, and the Director of the UF Interdisciplinary Microsystems Group (IMG). He has co-authored over 180 refereed journal and conference publications, and holds 19 U.S. patents. His research focuses on micro/nanostructured magnetic materials, magnetic microsystems, electromechanical transducers, and miniaturized power/energy systems.

Dr. Arnold is a member of Tau Beta Pi and Eta Kappa Nu. His research innovations have been recognized by the 2008 Presidential Early Career Award in Science and Engineering (PECASE) and the 2009 DARPA Young Faculty Award. He is an active participant in the magnetics and MEMS communities, with ongoing involvement in various conference committees and currently serving on the editorial boards of the *Journal of Micromechanics and Microengineering and Energy Harvesting and Systems*.

Luis Fernando Velásquez-García (M'09–SM'10) received the Mechanical Engineer and Civil Engineer degrees (*magna cum laude* and valedictorian of the School of Engineering in both cases) from the Universidad de Los Andes, Bogotá, Colombia, in 1998 and 1999, respectively, and the M.S. and Ph.D. degrees from the Massachusetts Institute of Technology (MIT), Cambridge, MA, USA, in 2001 and 2004, respectively.

In 2004, after completing his studies, he became a Post-Doctoral Associate at the Microsystems Technology Laboratories (MTL), MIT, where he was appointed as a Research Scientist, in 2005. Since 2009, he has been a Principal Scientist and Core Member with MTL. He is an Expert in micro and nanofabrication technologies. He leads the Micro- and Nano-enabled Multiplexed Scaled-down Systems Group, MIT, which conducts fundamental and applied research on devices and systems that exploit high-electric field phenomena (e.g., electrospray, gas ionization, field emission, X-rays, and plasmas) for space, energy, healthcare, manufacturing, and analytical applications. Currently, his work focuses on additively manufactured micro and nanosystems. He has authored more than 48 journal publications and 73 conference proceedings publications. He is the holder of 12 patents on MEMS/NEMS technologies.

Dr. Velásquez-García is a Full Member of Sigma Xi and a Senior Member of the American Institute of Aeronautics and Astronautics (AIAA). He has served as the Co-Chair of the 15th International Conference on Micro and Nanotechnology for Power Generation and Energy Conversion Applications (PowerMEMS 2015).